Biophysical Journal, Volume 98

Supporting Material

A Biophysically-based Mathematical Model for the Kinetics of Mitochondrial Na+-Ca2+ Antiporter

Ranjan K. Pradhan, Daniel A. Beard, and Ranjan K. Dash

Supporting Materials for "A Biophysically-based Mathematical Model for the Kinetics of Mitochondrial Na^+-Ca^{2+} Antiporter"

Ranjan K. Pradhan, Daniel A. Beard, and Ranjan K. Dash

Biotechnology and Bioengineering Center and Department of Physiology, Medical College of Wisconsin, Milwaukee, WI-53226

Address for Correspondence: Ranjan K. Dash, Ph.D., Biotechnology and Bioengineering Center, Medical College of Wisconsin, 8701 Watertown Plank Road, Milwaukee, WI 53226-6509, Phone: (414) 955-4497, Fax: (414) 955-6317, E-mail: rdash@mcw.edu

Appendix A: Membrane Potential Dependence of the Kinetic Parameters

The binding of $n\mathrm{Na}^+$ and $1\mathrm{Ca}^{2+}$ to the antiporter and translocation of $n\mathrm{Na}^+$ and $1\mathrm{Ca}^{2+}$ via the antiporter depends on the electrostatic field of the charged membrane. In order to account for this dependency, we assume here that the kinetics parameters K_{eq}, K_{Ne}, K_{Nx}, K_{Ce}, K_{Cx}, k_a and k_b depend on the electrostatic potential difference $\Delta\Psi$ across the membrane. Our approach is similar to that of Metelkin *et al.* (1) on the kinetic modeling of mitochondrial adenine nucleotide translocase (ANT) and Dash et al. (2) on the kinetic modeling of mitochondrial Ca^{2+} uniporter (CU). This approach is based on biophysical principles as well as laws of thermodynamics, electrostatics, and superposition. In this approach, it is assumed that the total value of the membrane potential is the sum of local electric potentials, each influencing the corresponding stages of $n\mathrm{Na}^+$ and $1\mathrm{Ca}^{2+}$ binding and translocation.

The assumed stages of $n\mathrm{Na}^+$ and $1\mathrm{Ca}^{2+}$ binding to the antiporter and $n\mathrm{Na}^+$ and $1\mathrm{Ca}^{2+}$ translocation via the antiporter for a $3\mathrm{Na}^+$:$1\mathrm{Ca}^{2+}$ electrogenic exchange ($n = 3$) are schematized in Figure A1. Every position of Na^+ or Ca^{2+} on the antiporter unit is characterized by an electric potential value. We assume here that the difference in potentials between the adjacent positions of Na^+ or Ca^{2+} is proportional to the total potential difference across the membrane. The sum of potential differences between the consecutive positions of Na^+ or Ca^{2+} is equal to the total potential difference across the membrane. Thus this approach divides the total drop in potential across the membrane into different elementary stages. The scheme described in Figure A1 illustrates the influence of such elementary potential drops on the rate of $3\mathrm{Na}^+$:$1\mathrm{Ca}^{2+}$ antiporter operation. Values of the potential drops are marked for all elementary stages of the scheme.

Equilibrium Constant: As a cycle of antiporter operation for a $n\mathrm{Na}^+$:$1\mathrm{Ca}^{2+}$ exchange involves translocation of n elementary positive charges ($n\mathrm{Na}^+$) into the matrix and two elementary positive charges ($1\mathrm{Ca}^{2+}$) out of the matrix, the dependence of the equilibrium constant K_{eq} on the membrane potential $\Delta\Psi$ can be expressed as (Nernst equation)

$$K_{eq} = \exp[(nZ_{Na} - Z_{Ca}) \cdot \Delta\Phi], \quad \Delta\Phi = F\Delta\Psi / RT, \tag{A1}$$

where F, R, and T denote the Faraday's constant, ideal gas constant, and absolute temperature, respectively; $Z_{Ca} = 2$ is the valence of Ca^{2+} and $Z_{Na} = 1$ is the valence of Na^+; $\Delta\Phi$ is the non-

dimensional potential difference across the membrane. In the absence of electric field ($\Delta\Psi = 0$), or for a $2Na^+$:$1Ca^{2+}$ electroneutral exchange, $K_{eq} = 1$.

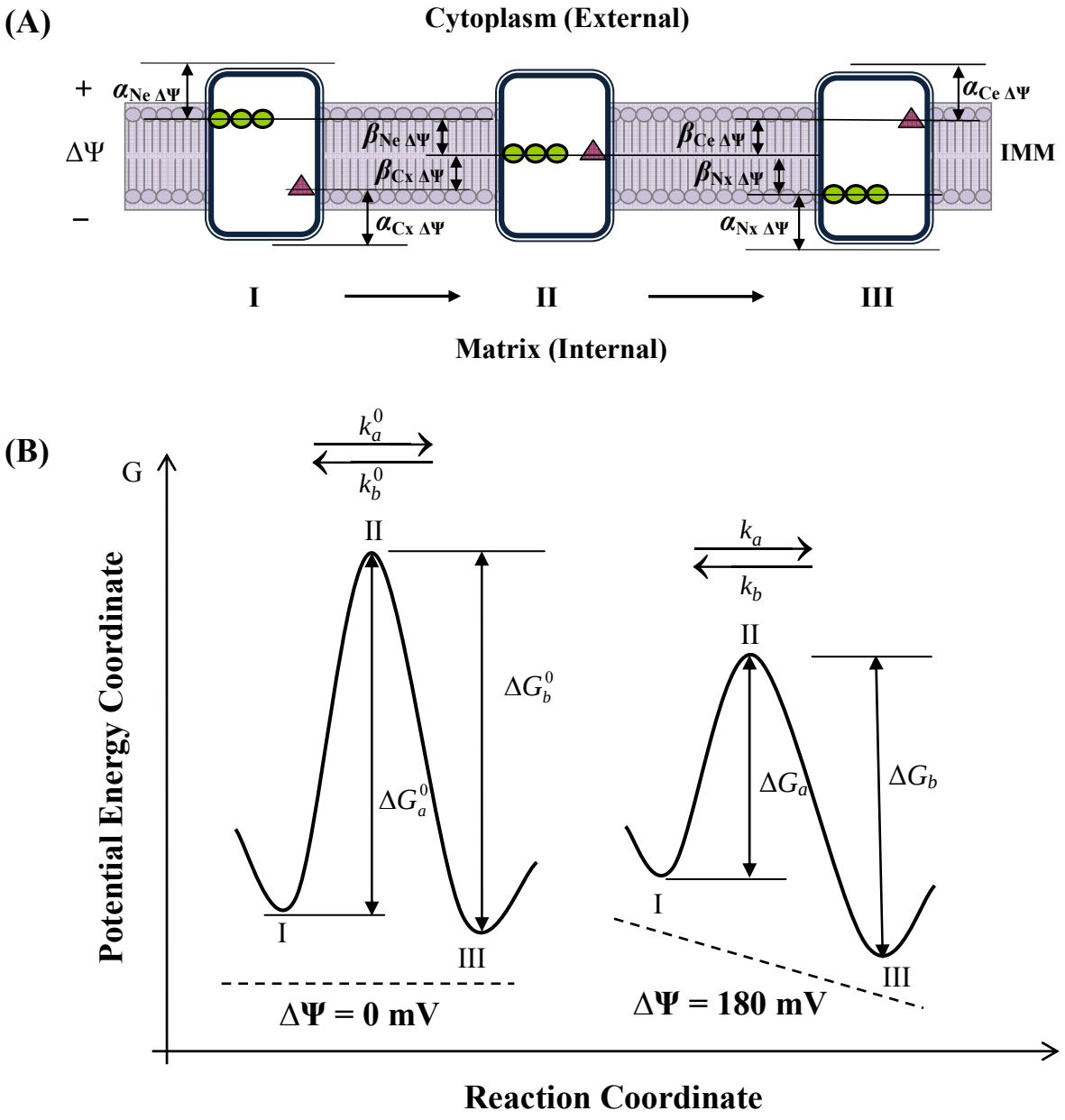

Figure A1: Free-energy barrier formalism for Na^+ influx/Ca^{2+} efflux via the $3Na^+$-$1Ca^{2+}$ antiporter. (A:I-III) The consecutive states of $3Na^+$ (circle) and $1Ca^{2+}$ (triangle) bound antiporter functional unit in the process of Na^+-Ca^{2+} exchange that is used to derive the dependence of the kinetic parameters on the membrane potential $\Delta\Psi$; α_{Ne} (α_{Ce}) represents the ratio of potential difference between Na^+ (Ca^{2+}) bound at the site of antiporter facing the external side of the IMM and Na^+ (Ca^{2+}) in the bulk phase to the total $\Delta\Psi$; α_{Nx} (α_{Cx}) represents the ratio of potential difference between Na^+ (Ca^{2+}) bound at the site of antiporter facing the internal side of the IMM and Na^+ (Ca^{2+}) in the bulk phase to the total $\Delta\Psi$; β_{Ne} (β_{Ce}) is the displacement of external Na^+ (Ca^{2+}) from the coordinate of maximum potential barrier; β_{Nx} (β_{Cx}) is the displacement of inter-

nal Na^+ (Ca^{2+}) from the coordinate of maximum potential barrier. (B) The potential energy barrier profile along the reaction coordinate that is used to derive the $\Delta\Psi$-dependence of the rate constants. The dashed line shows the profile of the potential created by the electric field of the charged membrane. The points I, II, and III correspond to the $3Na^+$ and $1Ca^{2+}$ bound antiporter states depicted in the upper panel (A). The rate constants k_a and k_b are related to the changes in potential energy (Gibbs free energy) ΔG_a and ΔG_b. In the absence of electric field ($\Delta\Psi = 0$ mV), the heights of free energy barriers in the forward and reverse directions are equal when the dissociation constants for the binding of external and internal Na^+ and Ca^{2+} to the antiporter are equal: $\Delta G_a^0 = \Delta G_b^0 = \Delta G^0$ if and only if $K_{Ne}^0 = K_{Nx}^0 = K_N^0$ and $K_{Cx}^0 = K_{Ce}^0 = K_C^0$.

Dissociation Constants: To derive the dependence of the dissociation constants of Na^+ and Ca^{2+} binding to the antiporter on the membrane potential $\Delta\Psi$, let us first consider the binding of external Na^+ and Ca^{2+} to the antiporter. The changes in Gibbs free energies for n binding reactions of external Na^+ and one binding reaction of external Ca^{2+} are given by

$$\begin{aligned}\Delta\mu_{Ne,p} &= \Delta\mu_{Ne,p}^0 + Z_{Na}\alpha_{Ne}F\Delta\Psi + RT\ln\left([E(p-1)Na_e^+][Na^+]_e/[EpNa_e^+]\right);\ p = 1,2,...n,\\ \Delta\mu_{Ce} &= \Delta\mu_{Ce}^0 + Z_{Ca}\alpha_{Ce}F\Delta\Psi + RT\ln\left([E][Ca^{2+}]_e/[ECa_e^{2+}]\right),\end{aligned} \quad \text{(A2)}$$

where $\Delta\mu_{Ne,p}^0$ and $\Delta\mu_{Ce}^0$ are the changes in standard Gibbs free energies of pth external Na^+ and one external Ca^{2+} binding reactions, respectively. The parameter α_{Ne} is the ratio of potential difference between Na^+ bound to the site of antiporter facing the cytoplasmic side of the IMM and Na^+ in the bulk phase to the total membrane potential $\Delta\Psi$ ($\Delta\Psi = \Psi_e - \Psi_x$; outside potential minus inside potential; so $\Delta\Psi$ is positive). Similarly, α_{Ce} is the ratio of potential difference between Ca^{2+} bound to the site of antiporter facing the cytoplasmic side of the IMM and Ca^{2+} in the bulk phase to the total membrane potential $\Delta\Psi$. An assumption inherent in this model is that all Na^+ binding sites on the antiporter are at equal distance from the bulk medium. At equilibrium ($\Delta\mu_{Ne,p} = 0$ and $\Delta\mu_{Ce} = 0$), Eq. (A2) gives

$$\begin{aligned}K_{Ne,p} &= \left([E(p-1)Na_e^+][Na^+]_e/[EpNa_e^+]\right)_{eq} = K_{Ne,p}^0\exp(-Z_{Na}\alpha_{Ne}\Delta\Phi);\ p = 1,2,...n,\\ K_{Ce} &= \left([E][Ca^{2+}]_e/[ECa_e^{2+}]\right)_{eq} = K_{Ce}^0\exp(-Z_{Ca}\alpha_{Ce}\Delta\Phi),\end{aligned} \quad \text{(A3)}$$

where $K_{Ne,p}^0 = K_{Ne,p}(\Delta\Psi = 0) = \exp(-\Delta\mu_{Ne,p}^0/RT)$ and $K_{Ce}^0 = K_{Ce}(\Delta\Psi = 0) = \exp(-\Delta\mu_{Ce}^0/RT)$. This indicates that the dissociation constants associated with the binding of external Na^+ as well as external Ca^{2+} to the antiporter are reduced (i.e., making the association easier) when $\Delta\Psi > 0$, provided α_{Ne} and α_{Ce} are positive.

Similarly, for the binding of internal Na^+ and Ca^{2+} to the antiporter, we have

$$\begin{aligned}K_{Nx,p} &= \left([(p-1)Na_x^+E][Na^+]_x/[pNa_x^+E]\right)_{eq} = K_{Nx,p}^0\exp(+Z_{Na}\alpha_{Nx}\Delta\Phi);\ p = 1,2,...n,\\ K_{Cx} &= \left([E][Ca^{2+}]_x/[Ca_x^{2+}E]\right)_{eq} = K_{Cx}^0\exp(+Z_{Ca}\alpha_{Cx}\Delta\Phi),\end{aligned} \quad \text{(A4)}$$

where $K_{Nx,p}^0 = K_{Nx,p}(\Delta\Psi = 0) = \exp(+\Delta\mu_{Nx,p}^0/RT)$ and $K_{Cx}^0 = K_{Cx}(\Delta\Psi = 0) = \exp(+\Delta\mu_{Cx}^0/RT)$; $\Delta\mu_{Nx,p}^0$ and $\Delta\mu_{Cx}^0$ are the standard changes in Gibbs free energies of n internal Na^+ and one internal Ca^{2+} binding reactions, respectively. The parameter α_{Nx} is the ratio of potential difference between Na^+ bound at the site of antiporter facing the matrix side of the IMM and Na^+ in the bulk

phase to the total membrane potential $\Delta\Psi$. Similarly, α_{Cx} is the ratio of potential difference between Ca^{2+} bound at the site of antiporter facing the matrix side of the IMM and Ca^{2+} in the bulk phase to the total membrane potential $\Delta\Psi$. In contrast to $K_{Ne,p}$ and K_{Ce}, the dissociation constants $K_{Nx,p}$ and K_{Cx} for binding of internal Na^+ and internal Ca^{2+} to the antiporter are increased (i.e., making the association difficult) when $\Delta\Psi > 0$, provided α_{Nx} and α_{Cx} are positive.

In any of the models derived in the paper (Model 1, Model 2, and Model 3), the dissociation constants K_{Ne}, K_{Nx}, K_{Ce}, and K_{Cx} can be obtained from Eqs. (A3) and (A4) as

$$\begin{aligned} K_{Ne} &= K_{Ne}^0 \exp(-\alpha_{Ne} Z_{Na} \Delta\Phi), \quad K_{Nx} = K_{Nx}^0 \exp(+\alpha_{Nx} Z_{Na} \Delta\Phi), \\ K_{Ce} &= K_{Ce}^0 \exp(-\alpha_{Ce} Z_{Ca} \Delta\Phi), \quad K_{Cx} = K_{Cx}^0 \exp(+\alpha_{Cx} Z_{Ca} \Delta\Phi). \end{aligned} \tag{A5}$$

For simplicity and reducing the number of unknown biophysical parameters, we assume here that $\alpha_{Ne} = \alpha_{Ce} = \alpha_e$ and $\alpha_{Nx} = \alpha_{Cx} = \alpha_x$, that is, the Na^+ and Ca^{2+} binding sites on the antiporter are located at equal distances from the bulk phase on either side of the IMM. Thus, the four dissociation constants K_{Ne}, K_{Nx}, K_{Ce} and K_{Cx} are fully characterized by six unknown parameters K_{Ne}^0, K_{Ce}^0, K_{Nx}^0, K_{Cx}^0, α_e and α_x, increasing the total number of unknown parameters by two. For positive α_e and α_x, the dissociation constants of Na^+ and Ca^{2+} binding tend to decrease on the outside and increase on the inside of the IMM. Also note here that K_{Ne}^0 and K_{Ce}^0 can be equal to/distinct from K_{Nx}^0 and K_{Cx}^0, respectively (see Case 1 and Case 2 in the paper).

Rate Constants: The dependence of the rate constants k_a and k_b on the membrane potential $\Delta\Psi$ during conformational changes of the antiporter complexes $Ca_x^{2+} mH_x^+ E nNa_e^+$ and $nNa_x^+ E mH_e^+ Ca_e^{2+}$ can be accounted for by using Eyring's free energy barrier theory for absolute reaction rates (3-5). For simplicity, we assume here that the free energy profile for the translocation of nNa^+ and $1Ca^{2+}$ across the membrane (the limiting stage) is a single barrier (Figure A1B), and the translocation is a jump over the barrier from one potential well to another. We define the reaction coordinate for Na^+ translocation as the coordinate from Na^+ bound at the external side to Na^+ bound at the internal side of the membrane along the direction of Na^+ translocation. Similarly, the reaction coordinate for Ca^{2+} translocation is defined as the coordinate from Ca^{2+} bound at the internal side to Ca^{2+} bound at the external side of the membrane along the direction of Ca^{2+} translocation. The local maximum or peak (State II) of the free energy profile corresponds to the barrier that impends the nNa^+ and $1Ca^{2+}$ translocation, while the local minima (States I and III) corresponds to the $Ca_x^{2+} mH_x^+ E nNa_e^+$ and $nNa_x^+ E mH_e^+ Ca_e^{2+}$ states on either side of the membrane. The nNa^+ and $1Ca^{2+}$ exchange rate is determined by the probability of the antiporter to translocate nNa^+ for $1Ca^{2+}$ from one binding site to the other in opposite direction, which depends on the height of the free energy barrier, which in turn depends on $\Delta\Psi$, as shown in Figure A1B.

According to Eyring's free energy barrier theory, the rate (k) at which an ion can jump from one binding site to other is given by

$$k = (\kappa_B T / h) \exp\left(-\Delta G / RT\right), \tag{A6}$$

where ΔG is the height of the free energy barrier; k_B is Boltzmann's constant; h is Planck's constant; and T is the absolute temperature. In this model, the free energy barrier heights (State II to States I and III) can be defined by,

$$\Delta G_a = \Delta G_a^0 - nZ_{\mathrm{Na}}\beta_{\mathrm{Ne}}F\Delta\Psi + Z_{\mathrm{Ca}}\beta_{\mathrm{Cx}}F\Delta\Psi,$$
$$\Delta G_b = \Delta G_b^0 + nZ_{\mathrm{Na}}\beta_{\mathrm{Nx}}F\Delta\Psi - Z_{\mathrm{Ca}}\beta_{\mathrm{Ce}}F\Delta\Psi, \tag{A7}$$

where

$$\beta_{\mathrm{Ne}} = \beta_{\mathrm{Ne}} + \sum_j \frac{\beta_{\mathrm{e,j}}Z_{\mathrm{j}}}{nZ_{\mathrm{Na}}},\ \beta_{\mathrm{Cx}} = \beta_{\mathrm{Cx}} + \sum_j \frac{\beta_{\mathrm{x,j}}Z_{\mathrm{j}}}{Z_{\mathrm{Ca}}},$$
$$\beta_{\mathrm{Nx}} = \beta_{\mathrm{Nx}} + \sum_j \frac{\beta_{\mathrm{x,j}}Z_{\mathrm{j}}}{nZ_{\mathrm{Na}}},\ \beta_{\mathrm{Ce}} = \beta_{\mathrm{Ce}} + \sum_j \frac{\beta_{\mathrm{e,j}}Z_{\mathrm{j}}}{Z_{\mathrm{Ca}}}. \tag{A8}$$

In Eq. (A7), ΔG_a^0 and ΔG_b^0 are the free energy barrier heights in the absence of electric field ($\Delta\Psi$ = 0 mV); β_{Ne} and β_{Ce} are the displacements of external Na^+ and Ca^{2+} (State I and State III) from the coordinate of maximum potential barrier (State II); β_{Nx} and β_{Cx} are the displacements of internal Na^+ and Ca^{2+} (State III and State I) from the coordinate of maximum potential barrier (State II). Note here that $\Delta G_a^0 = \Delta G_b^0 = \Delta G^0$ subject to conditions $K_{\mathrm{Ne}}^0 = K_{\mathrm{Nx}}^0 = K_{\mathrm{N}}^0$ and $K_{\mathrm{Ce}}^0 = K_{\mathrm{Cx}}^0 = K_{\mathrm{C}}^0$. For simplicity, the effects of the displacements of other elementary charges that constitute the antiporter on the rate of conformational change has been lumped into the biophysical parameters β_{Ne}, β_{Nx}, β_{Ce} and β_{Cx}, as shown in Eq. (A8). In Eq. (A8), the parameter Z_j is the valence of the jth charged species of the antiporter and $\beta_{\mathrm{e,j}}$ and $\beta_{\mathrm{x,j}}$ are the corresponding displacements from the external and internal sides of the antiporter.

It is evident from Eq. (A7) that the Na^+ ions tend to decrease the height of the barrier in the inward direction, but increase the height of the barrier in the outward direction, when $\Delta\Psi > 0$ (see Figure A1B). Similarly, the Ca^{2+} ions tend to increase the height of the barrier in the inward direction, but decrease the height of the barrier in the outward direction, when $\Delta\Psi > 0$. In other words, it becomes easier for the Na^+ (Ca^{2+}) ions to cross the barrier in the inward (outward) direction, but more difficult for the Na^+ (Ca^{2+}) ions to exit (enter) the matrix in the presence of a positive membrane potential, measured from outside to inside. Now, substituting Eq. (A7) into Eq. (A6), we obtain the rate constants of $n$$Na^+$ and 1Ca^{2+} exchange as

$$k_a = k_a^0 \exp\left[(+n\beta_{\mathrm{Ne}}Z_{\mathrm{Na}} - \beta_{\mathrm{Cx}}Z_{\mathrm{Ca}})\Delta\Phi\right],$$
$$k_b = k_b^0 \exp\left[(-n\beta_{\mathrm{Nx}}Z_{\mathrm{Na}} + \beta_{\mathrm{Ce}}Z_{\mathrm{Ca}})\Delta\Phi\right], \tag{A9}$$

where $k_a^0 = (\kappa_B T/h)\exp(-\Delta G_a^0/RT)$ and $k_b^0 = (\kappa_B T/h)\exp(-\Delta G_b^0/RT)$ are the forward and reverse rate constants when $\Delta\Psi$ = 0 mV. For simplicity and to reducing the number of unknown biophysical parameters, we assume here that the displacements of Na^+ and Ca^{2+} ions (State I and State III) from the coordinate of maximum potential barrier (State II) are the same on either side of the IMM: $\beta_{\mathrm{Ne}} = \beta_{\mathrm{Ce}} = \beta_{\mathrm{e}}$ and $\beta_{\mathrm{Nx}} = \beta_{\mathrm{Cx}} = \beta_{\mathrm{x}}$. Thus, the two rate constants k_a and k_b are fully characterized by four unknown parameters k_a^0, k_b^0, β_{e} and β_{x}, increasing the total number of unknown parameters by two.

Appendix B: Model of Mitochondrial Na^+-Ca^{2+} Antiporter for $2Na^+$:$1Ca^{2+}$ Stoichiometry

This appendix presents three different kinetic models of mitochondrial $2Na^+$-$1Ca^{2+}$ antiporter based on the proposed kinetic mechanism shown in Figure B1. The parameterization of these three kinetic models (Model 1: fully cooperativity, Model 2: partial cooperativity, and Model 3: no cooperativity) under two different model assumptions regarding the magnitudes of the binding constants of Na^+ and Ca^{2+} to the antiporter at the inside and outside of the membrane (Case 1 and Case 2) is done using the experimental data of Paucek and Jaburek (6). The model equations can be easily derived from Eqs. (10-11) with $n = 2$, and hence are not shown here. The model specifications and different model assumptions are the same as mentioned in the paper. The fitting of all three models to the experimental data are shown in Figures B2 and B3. The estimated model parameter values are summarized in Table B1.

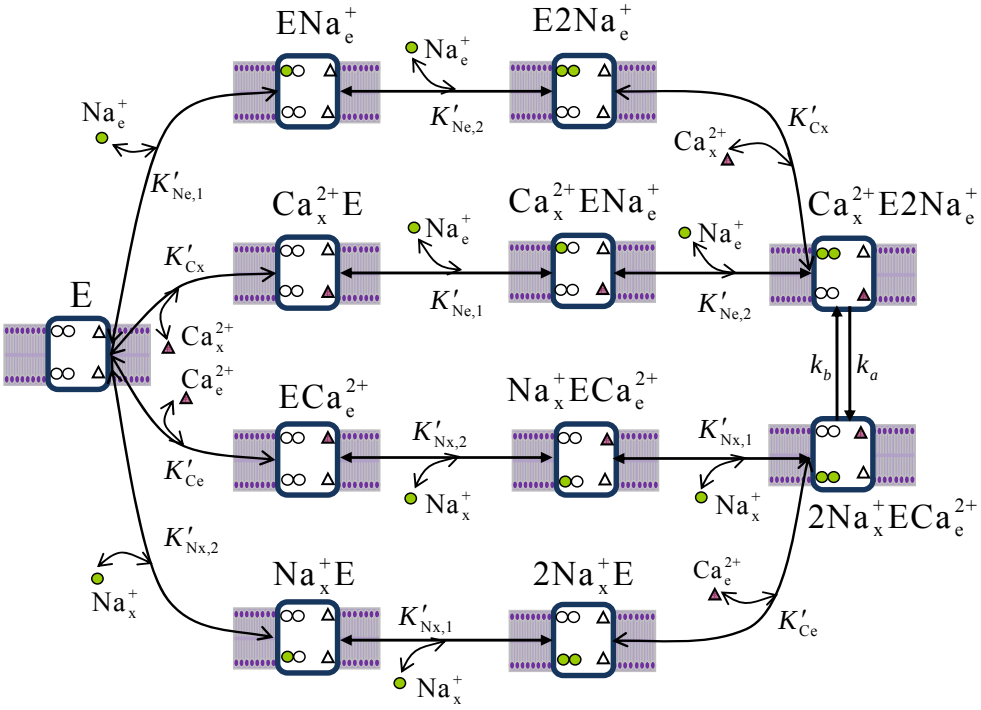

Figure B1: Proposed kinetic mechanism of Na^+-dependent Ca^{2+} efflux from mitochondria via Na^+-Ca^{2+} antiporter with a presumed $2Na^+$:$1Ca^{2+}$ stochiometry. The antiporter functional unit (E) is assumed to have two binding sites for Na^+ and one binding site for Ca^{2+} facing either side of the inner mitochondrial membrane (IMM). In one process, two Na^+ ions from the external (cytoplasmic) side of the IMM ($2\,Na_e^+$) first cooperatively bind to the unbound antiporter E in two consecutive steps forming the antiporter complex $E2Na_e^+$. Then, a Ca^{2+} ion from the internal (matrix) side of the IMM (Ca_x^{2+}) binds to the complex $E2Na_e^+$ forming the complex $Ca_x^{2+}E2Na_e^+$. In another process, a Ca^{2+} ion from the matrix side (Ca_x^{2+}) first binds to the unbound antiporter E to form the antiporter complex $Ca_x^{2+}E$. Then, two Na^+ ions from the cytoplasmic side ($2\,Na_e^+$) cooperatively bind to the complex $Ca_x^{2+}E$ in two consecutive steps to form the complex $Ca_x^{2+}E2Na_e^+$. The complex $Ca_x^{2+}E2Na_e^+$ that is formed via these two distinct processes then un-

dergoes conformational changes (or flips upside down) to form the complex $2Na_x^+ECa_e^{2+}$. The complex $2Na_x^+ECa_e^{2+}$ undergoes the reverse processes, where it dissociates in two distinct processes to form two Na^+ ions in the matrix side of the IMM ($2\,Na_x^+$) and one Ca^{2+} ion in the cytoplasmic side of the IMM (Ca_e^{2+}), in addition to the formation of the unbound antiporter E. $K'_{Ne,1}$, $K'_{Nx,1}$, $K'_{Ne,2}$, $K'_{Nx,2}$, K'_{Ce} and K'_{Cx} are the apparent dissociation constants associated with the binding of external and internal Na^+ and Ca^{2+} to the antiporter. The exchange of $2Na^+$ for $1Ca^{2+}$ via the interconversion mechanism $Ca_x^{2+}E2Na_e^+ \leftrightarrow 2Na_x^+ECa_e^{2+}$ is limited by the forward and reverse rate constants k_a and k_b which are independent of IMM potential $\Delta\Psi$.

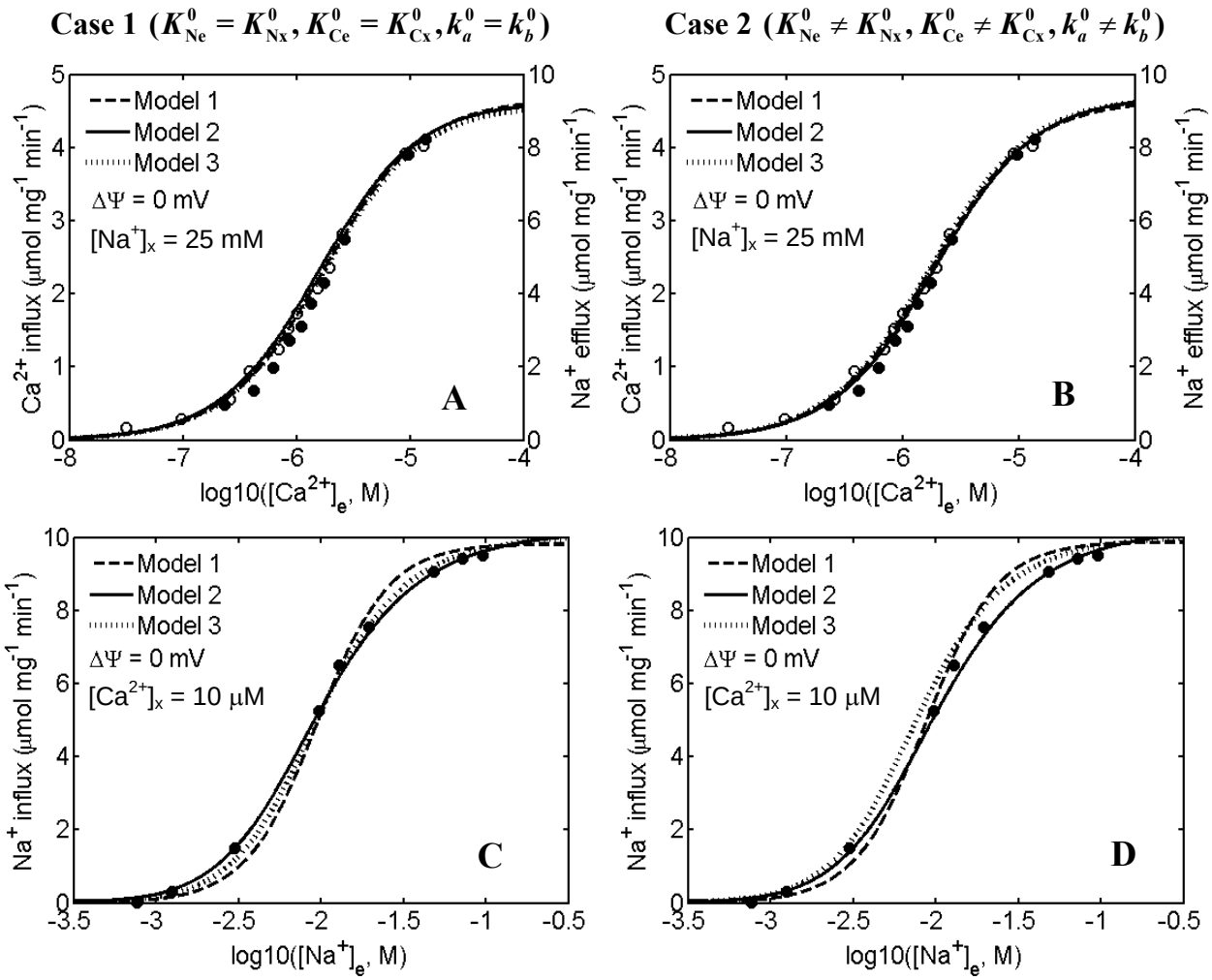

Figure B2: Comparison of mitochondrial $2Na^+$-$1Ca^{2+}$ antiporter models (lines) to the experimental data (points) of Paucek and Jaburek (6) on the kinetics of Na^+ and Ca^{2+} fluxes via the antiporter with fixed external pH. Shown are the best fits of three different kinetic models (Model 1, Model 2, and Model 3) under two different model assumptions (Case 1, left panel: A,C and Case 2, right panel: B,D) to the kinetic data of Paucek and Jaburek in which the initial rates of Ca^{2+} influx (Na^+ efflux) with variations in external $[Ca^{2+}]$ (internal $[Na^+]$ = 25 mM, external $[Na^+]$ = 0 mM, internal $[Ca^{2+}]$ = 0 μM, internal pH = 7.3, and external pH = 7.3) (A,B:

upper panel) and the initial rates of Na^+ influx (Ca^{2+} efflux) with variations in external [Na^+] (internal [Na^+] = 0 mM, internal [Ca^{2+}] = 10 μM, external [Ca^{2+}] = 0 μM, internal pH = 7.3, and external pH = 7.3) (C,D: lower panel) were measured in proteoliposomes reconstituted with purified Na^+-Ca^{2+} antiporters of beef heart mitochondria. The models were fitted to the data by setting the membrane potential $\Delta\Psi$ = 0 mV, in consistent with the experimental protocol. The dashed lines are the simulations from Model 1 ($K'_{Ne,1} >> 1$ μM, $K'_{Ne,2} << 1$ μM and $K'_{Nx,1} >> 1$ μM, $K'_{Nx,2} << 1$ μM such that $K'_{Ne,1}K'_{Ne,2} = K'^2_{Ne}$ and $K'_{Nx,1}K'_{Nx,2} = K'^2_{Nx}$; fully cooperativity), the solid lines are the simulations from Model 2 ($K'_{Ne,1} = K'_{Ne,2} = K'_{Ne}$ and $K'_{Nx,1} = K'_{Nx,2} = K'_{Nx}$; partial cooperativity), and the dotted lines are the simulations from Model 3 ($K'_{Ne,1} = 2K'_{Ne}$, $K'_{Ne,2} = K'_{Ne}/2$ and $K'_{Nx,1} = 2K'_{Nx}$, $K'_{Nx,2} = K'_{Nx}/2$; no cooperativity) for both the conditions (Case 1: $K^0_{Ne} = K^0_{Nx}$, $K^0_{Ce} = K^0_{Cx}$ and $k^0_a = k^0_b$ and Case 2: $K^0_{Ne} \neq K^0_{Nx}$, $K^0_{Ce} \neq K^0_{Cx}$ and $k^0_a \neq k^0_b$). The model parameter values are as given in Table B1.

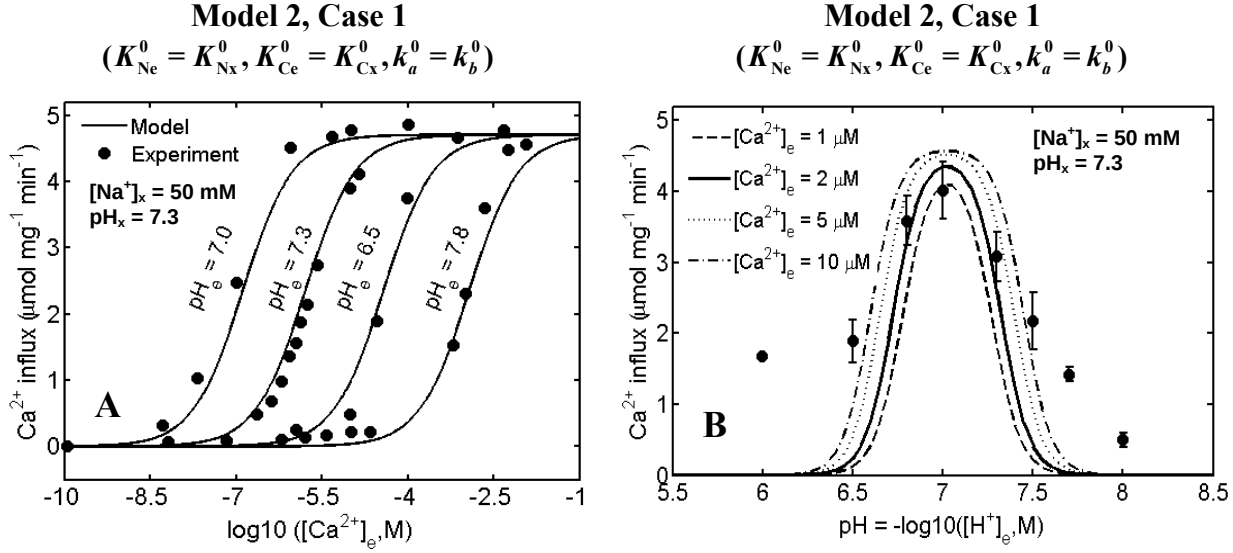

Figure B3: Comparison of mitochondrial $2Na^+$-$1Ca^{2+}$ antiporter models (lines) to the experimental data (points) of Paucek and Jaburek (6) on the kinetics of Na^+ and Ca^{2+} fluxes via the antiporter with varying external pH. Shown are the best fits of the best kinetic model (Model 2, Case 1) to the kinetic data of Paucek and Jaburek in which the initial rates of Ca^{2+} influx (Na^+ efflux) with (A) variations in external [Ca^{2+}] at four different levels of external pH (internal [Na^+] = 50 mM, external [Na^+] = 0 mM, internal [Ca^{2+}] = 0 μM, internal pH = 7.3, and external pH = 7.0, 7.3, 6.5 and 7.8), and (B) variations in external pH and fixed external [Ca^{2+}] (internal [Na^+] = 50 mM, external [Na^+] = 0 mM, internal [Ca^{2+}] = 0 μM, external [Ca^{2+}] = 2 μM, and internal pH = 7.3) were measured in proteoliposomes reconstituted with purified Na^+-Ca^{2+} antiporters of beef heart mitochondria. Also shown in plot B are the model simulations of the initial rates of Ca^{2+} influx (Na^+ efflux) with variations in external pH at four different levels of external [Ca^{2+}] (1, 2, 5 and 10 μM) with other experimental conditions remaining the same. The model specifications for Model 2 and model assumptions for Case 1 are the same as in Figure B2. The model was fitted to the data by setting the membrane potential $\Delta\Psi$ = 0 mV, in consistent with the experimental protocol. The model parameter values are given in Table B1.

Table B1: The estimated parameter values in the kinetic models of mitochondrial $2Na^{+}$-$1Ca^{2+}$ antiporter from the experimental data of Paucek and Jaburek (6). The kinetic parameters satisfy the constraint: $(k_a^0 / k_b^0)(K_{\mathrm{Ce}}^0 / K_{\mathrm{Cx}}^0)(K_{\mathrm{Nx}}^0 / K_{\mathrm{Ne}}^0)^2 = 1$. The biophysical parameters are chosen as $\alpha_e = \alpha_x = \alpha = 0$ and $\beta_e = \beta_x = \beta = 0.5$. The rate constants are in the units of μmol/mg/min and the dissociation constants are in the units of molar (M). Reference 'r1' corresponds to Figure B2 (A,B) and reference 'r2' corresponds to Figure B2 (C,D).

Parameter	Values for Model 1		Values for Model 2		Values for Model 3		Reference
	Case 1 ($K_{\mathrm{Ne}}^0 = K_{\mathrm{Nx}}^0$, $K_{\mathrm{Ce}}^0 = K_{\mathrm{Cx}}^0$)	Case 2 ($K_{\mathrm{Ne}}^0 \neq K_{\mathrm{Nx}}^0$, $K_{\mathrm{Ce}}^0 \neq K_{\mathrm{Cx}}^0$)	Case 1 ($K_{\mathrm{Ne}}^0 = K_{\mathrm{Nx}}^0$, $K_{\mathrm{Ce}}^0 = K_{\mathrm{Cx}}^0$)	Case 2 ($K_{\mathrm{Ne}}^0 \neq K_{\mathrm{Nx}}^0$, $K_{\mathrm{Ce}}^0 \neq K_{\mathrm{Cx}}^0$)	Case 1 ($K_{\mathrm{Ne}}^0 = K_{\mathrm{Nx}}^0$, $K_{\mathrm{Ce}}^0 = K_{\mathrm{Cx}}^0$)	Case 2 ($K_{\mathrm{Ne}}^0 \neq K_{\mathrm{Nx}}^0$, $K_{\mathrm{Ce}}^0 \neq K_{\mathrm{Cx}}^0$)	
k_a^0	5.2, 5.75	5.1, 5.71	5.9, 5.9	5.81, 6.0	5.8, 5.9	5.3, 5.83	r1, r2
k_b^0	5.2, 5.75	5.2, 5.82	5.9, 5.9	5.90, 6.1	5.8, 5.9	5.4, 5.94	r1, r2
K_{Ne}^0	8.86×10^{-3}	8.20×10^{-3}	5.61×10^{-3}	5.89×10^{-3}	7.10×10^{-3}	5.76×10^{-3}	r1, r2
K_{Nx}^0	8.86×10^{-3}	7.93×10^{-3}	5.61×10^{-3}	5.60×10^{-3}	7.10×10^{-3}	5.56×10^{-3}	r1, r2
K_{Ce}^0	2.29×10^{-9}	2.29×10^{-9}	2.27×10^{-9}	2.26×10^{-9}	2.10×10^{-9}	2.30×10^{-9}	r1, r2
K_{Cx}^0	2.29×10^{-9}	2.10×10^{-9}	2.27×10^{-9}	2.01×10^{-9}	2.10×10^{-9}	2.10×10^{-9}	r1, r2
K'^0_{Ce} (pH=7.0)	1.37×10^{-7}	1.38×10^{-7}	1.30×10^{-7}	1.45×10^{-7}	1.34×10^{-7}	1.42×10^{-7}	r1, r2
K'^0_{Ce} (pH=7.3)	1.70×10^{-6}	1.70×10^{-6}	1.56×10^{-6}	1.88×10^{-6}	1.68×10^{-6}	1.71×10^{-6}	r1, r2
K'^0_{Ce} (pH=6.5)	3.92×10^{-5}	4.00×10^{-5}	3.76×10^{-5}	4.16×10^{-5}	3.94×10^{-5}	4.23×10^{-5}	r1, r2
K'^0_{Ce} (pH=7.8)	1.22×10^{-3}	1.22×10^{-3}	1.18×10^{-3}	1.37×10^{-3}	1.22×10^{-3}	1.23×10^{-3}	r1, r2
K'^0_{Cx} (pH=7.3)	1.70×10^{-6}	1.56×10^{-6}	1.56×10^{-6}	1.67×10^{-6}	1.68×10^{-6}	1.56×10^{-6}	r1, r2
K_{H1}	6.47×10^{-8}	6.45×10^{-8}	6.51×10^{-8}	6.39×10^{-8}	6.37×10^{-8}	6.39×10^{-8}	r1, r2
K_{H2}	1.40×10^{-7}	1.40×10^{-7}	1.38×10^{-7}	1.43×10^{-7}	1.42×10^{-7}	1.40×10^{-7}	r1, r2

Appendix C: Integrated Modeling of Mitochondrial Bioenergetics and Ca^{2+} Handling

In spite of large number of kinetic studies (6-10), the stoichiometry of mitochondrial Na^+-Ca^{2+} antiporter is not well established. Furthermore, the antiporter function under pathophysiological conditions (e.g., myocardial ischemia) is not well known. In a step towards understanding these aspects, the proposed model of mitochondrial Na^+-Ca^{2+} antiporter and our recently developed model of mitochondrial Ca^{2+} uniporter (2) is integrated to our existing model of mitochondrial bioenergetics and Ca^{2+} handling (11). The integrated model is then applied to characterize the stoichiometry of the antiporter as well as to predict the antiporter function with varying levels of external (cytosolic) pH that occur during pathophysiological conditions.

Characterization of the Stoichiometry of the *n*Na^+-1Ca^{2+}Antiporter:

This section presents the application of the proposed kinetic model of mitochondrial *n*Na^+-1Ca^{2+} antiporter to characterize the stoichiometry of the antiporter. For doing this, the best model of the antiporter (Model 2, Case 1; $n = 2$ or 3) is integrated into our recently developed computational model of mitochondrial bioenergetics and Ca^{2+} handling (11). The resulting integrated model is further modified by incorporating our recently developed biophysical model of mitochondrial Ca^{2+} uniporter (2), while keeping the other model components and equations the same, as reported in the previous Supplementary Material (11). The integrated model (with $n = 2$ and 3) is then applied to simulate the experimental data of Cox and Matlib (12) in which the time course of matrix free [Ca^{2+}] in purified respiring mitochondria from rabbit hearts with addition of varying levels of Na^+ to the extra-matrix buffer medium with the activity of mitochondrial Ca^{2+} uniporter blocked by ruthenium red. The result of this analysis is summarized in Figure C1. The integrated model with 3Na^+-1Ca^{2+} antiporter successfully describes the data, while the integrated model with 2Na^+-1Ca^{2+} antiporter deviates significantly from the data. This further validates our previous hypothesis that the stoichiometry of mitochondrial Na^+-Ca^{2+} antiporter is 3:1 (i.e., an electrogenic exchange of 3Na^+ for 1Ca^{2+} via the antiporter).

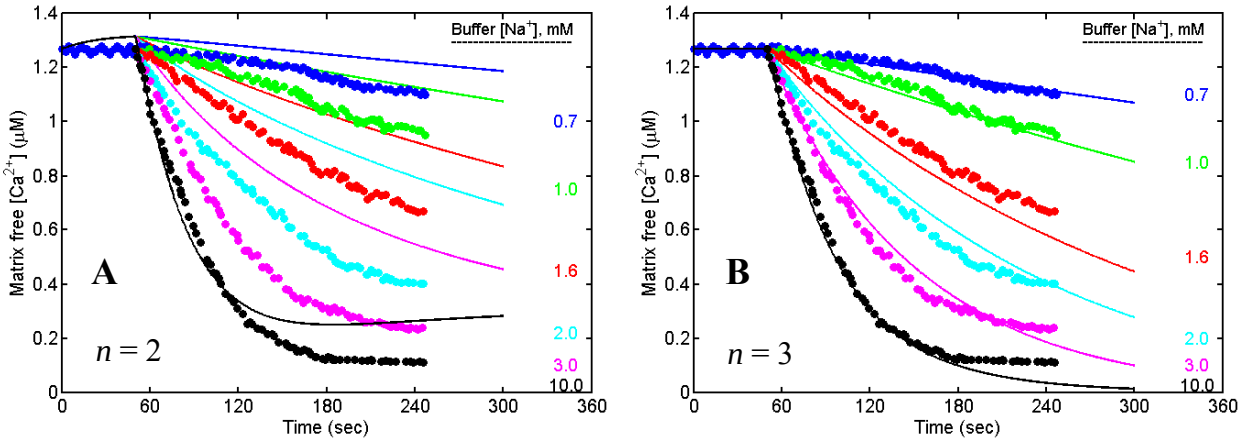

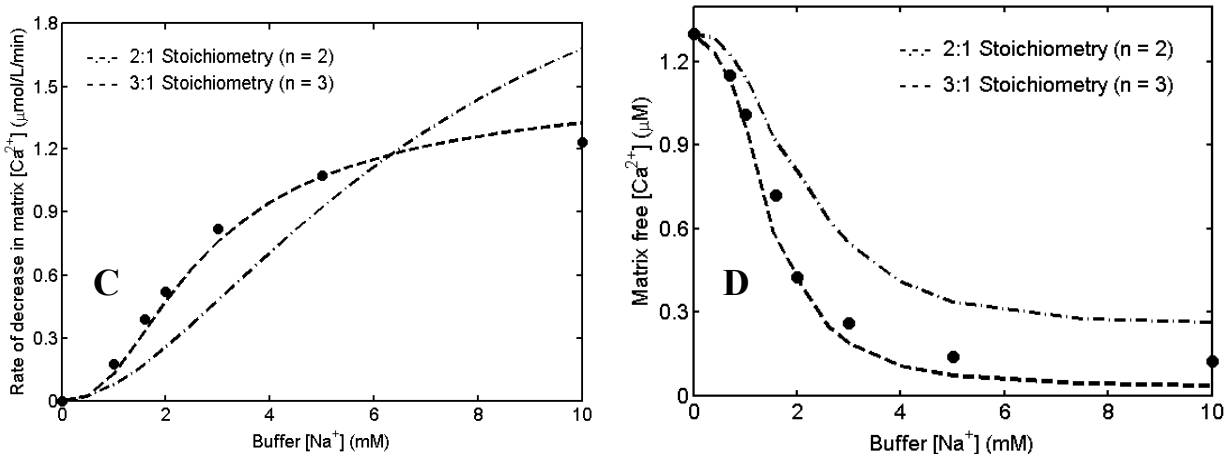

Figure C1: Characterization of the stoichiometry of mitochondrial nNa$^+$-1Ca^{2+} antiporter. Shown are the comparisons of the integrated model predictions (lines) to the experimental data (points) of Cox and Matlib (12) with both (A,C,D) 2Na$^+$-1Ca^{2+} and (B,C,D) 3Na$^+$-1Ca^{2+} antiporter models. The total buffer [Ca^{2+}] was fixed at 20 μM, corresponding to a free buffer [Ca^{2+}] of 0.15 μM with 50 μM of EGTA in the external buffer medium (external pH = 7.2). The antiporter model uses the same parameter values for K_{Ce}, K_{Cx}, K_{H1}, K_{H2}, α and β as estimated before (Tables 1 and B1), while the rate constants k_a and k_b and the dissociation constants K_{Ne} and K_{Nx} are varied to obtain the best fit of the model to the data on the dynamic of matrix free [Ca^{2+}] (Plots: A,B). The parameters K_{Ne} and K_{Nx} are found to be 1.6 mM for 3Na$^+$-1Ca^{2+} antiporter model and 4.4 mM for 2Na$^+$-1Ca^{2+} antiporter model. The rate constants k_a and k_b are found to be 7.8 nmol of Ca^{2+}/L/sec for 3Na$^+$-1Ca^{2+} antiporter model and 650 nmol of Ca^{2+}/L/sec for 2Na$^+$-1Ca^{2+} antiporter model. Plot C shows the comparisons of integrated model simulations to the initial rates of decrease of matrix free [Ca^{2+}] following addition of different levels of Na$^+$ to the external buffer medium, using both 2Na$^+$-1Ca^{2+} and 3Na$^+$-1Ca^{2+} antiporter models. Plot D shows the corresponding comparisons on the levels of matrix free [Ca^{2+}] after 3 min of Na$^+$ addition to the buffer medium.

Mitochondrial Ca^{2+} Dynamics during Pathophysiological Conditions:

In order to predict the effect of 3Na$^+$-1Ca^{2+} antiporter on mitochondrial Ca^{2+} regulation during pathophysiological states (high and low pH), the integrated model of mitochondrial bioenergetics and Ca^{2+} handling is used to simulate the dynamics of matrix free [Ca^{2+}] based on the experimental protocol of Cox and Matlib (12) with fixed external [Na$^+$] of 3 mM and different external pH (Ca^{2+} uniporter blocked) which is shown in Figure C2 (A). The corresponding dynamics of Na$^+$ influx (Ca^{2+} efflux) via the antiporter is shown in Figure C2 (B). The simulations with different external [Na$^+$] and fixed external pH of 7.2 is shown above in Figure C1 (B). These simulations show that the model is able to adequately predict the experimental data with external pH = 7.2, and the antiporter function is optimal at pH ≈ 7.0. However, at high and low pH (i.e., for pH < 6.5 and pH > 7.5), the model significantly deviates from the data. At these levels of pH, the Na$^+$-Ca^{2+} antiporter flux is significantly reduced due to the inhibition of the antiporter function by protons, resulting in significantly higher matrix free [Ca^{2+}] compared to pH around 7.0.

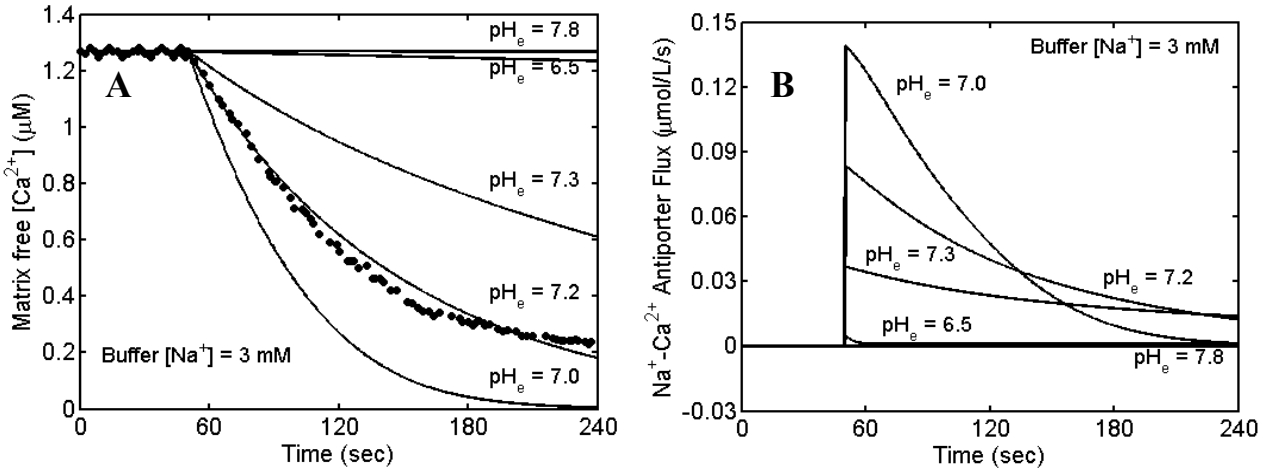

Figure C2: Effect of extra-matrix buffer pH variations on the dynamics of matrix free [Ca^{2+}] and Ca^{2+} efflux (Na^+ influx) via the $3Na^+$:$1Ca^{2+}$ antiporter. (Plot A) Shown are the integrated model simulations (lines) of the dynamics of matrix free [Ca^{2+}] at different levels of external pH (6.5, 7.0, 7.2, 7.3, 7.8) based on the experimental protocol of Cox and Matlib (12) in which the time course of matrix free [Ca^{2+}] were measured (points) following addition of varying levels of [Na^+] to the external buffer medium (external EGTA = 50 μM, external total [Ca^{2+}] = 20 μM, internal free [Ca^{2+}] = 1.27 μM, external pH = 7.2) in purified respiring mitochondria from rabbit hearts with the activity of Ca^{2+} uniporter blocked by ruthenium red (also see Figure C1). The data and corresponding model simulations are shown only for external [Na^+] = 3 mM. (Plot B) Shown are the integrated model simulations of the dynamics of Na^+-Ca^{2+} fluxes via the antiporter at different levels of external pH with the simulation protocol the same as in Plot A. The simulations are conducted by exclusively integrating the best $3Na^+$:$1Ca^{2+}$ antiporter model (Model 2, Case 1) to our previous model of mitochondrial bioenergetics and Ca^{2+} handling (11).

REFERENCES

1. Metelkin, E., I. Goryanin, and O. Demin. 2006. Mathematical modeling of mitochondrial adenine nucleotide translocase. *Biophys J* 90(2):423-432.
2. Dash, R.K., F. Qi, and D.A. Beard. 2009. A biophysically based mathematical model for the kinetics of mitochondrial calcium uniporter. *Biophys J* 96(4):1318-1332.
3. Keener, J.P., and J. Sneyd. 1998. Mathematical Physiology. Springer, New York.
4. Lauger, P. 1973. Ion transport through pores: a rate-theory analysis. *Biochim Biophys Acta* 311(3):423-441.
5. Woodbury, J.W. 1971. Eyring rate theory model of the current-voltage relationship of ion channels in excitable membranes. *In* Chemical Dynamics: Papers in Honor of Henry Eyring. Hirschfelder J, editor. John Wiley and Sons Inc., New York.
6. Paucek, P., and M. Jaburek. 2004. Kinetics and ion specificity of Na^+/Ca^{2+} exchange mediated by the reconstituted beef heart mitochondrial Na^+/Ca^{2+} antiporter. *Biochim Biophys Acta* 1659(1):83-91.

7. Brand, M.D. 1985. The stoichiometry of the exchange catalysed by the mitochondrial calcium/sodium antiporter. *Biochem J* 229(1):161-166.
8. Wingrove, D.E., and T.E. Gunter. 1986. Kinetics of mitochondrial calcium transport. II. A kinetic description of the sodium-dependent calcium efflux mechanism of liver mitochondria and inhibition by ruthenium red and by tetraphenylphosphonium. *J Biol Chem* 261(32):15166-15171.
9. Baysal, K., D.W. Jung, K.K. Gunter, T.E. Gunter, and G.P. Brierley. 1994. Na^+-dependent Ca^{2+} efflux mechanism of heart mitochondria is not a passive $Ca^{2+}/2Na^+$ exchanger. *Am J Physiol* 266(3 Pt 1):C800-808.
10. Jung, D.W., K. Baysal, and G.P. Brierley. 1995. The sodium-calcium antiport of heart mitochondria is not electroneutral. *J Biol Chem* 270(2):672-678.
11. Dash, R.K., and D.A. Beard. 2008. Analysis of cardiac mitochondrial Na^+-Ca^{2+} exchanger kinetics with a biophysical model of mitochondrial Ca^{2+} handling suggests a 3:1 stoichiometry. *J Physiol* 586(13):3267-3285.
12. Cox, D.A., and M.A. Matlib. 1993. A role for the mitochondrial Na^+-Ca^{2+} exchanger in the regulation of oxidative phosphorylation in isolated heart mitochondria. *J Biol Chem* 268(2):938-947.